Harmonic Current Suppression for PMSM Drives via Time-Shifting Harmonic Extraction

Zekai Lyu, *Member*, *IEEE*, Shuangxia Niu, *Senior Member*, *IEEE*, Haolan Zhan, *Student Member*, *IEEE*, Tao Wang, *Senior Member*, *IEEE*, Lijian Wu, *Senior Member*, *IEEE*, and K. T. Chau, *Fellow*, *IEEE*

***Abstract*—Multiple synchronous reference frame (MSRF) current control scheme is frequently utilized in permanent-magnet synchronous machine (PMSM) drive systems for harmonic current suppression. However, low-pass filters (LPFs) with relatively low cutoff frequencies are commonly used to separate the fundamental and the major current harmonic components, which can introduce significant delays in the control loop, degrading the system performance. To address this issue, this paper proposes a rapid and efficient harmonic current suppression scheme for PMSMs by incorporating a fast harmonic extraction method based on numerical calculation. For the separation of fundamental, 5th and 7th harmonic currents, the proposed method only requires the current data from three sampling moments for processing, essentially constituting a time-shifting operation. Then the current with different orders can be decoupled and transformed into different harmonic planes, and independent closed-loop control can be realized. Compared with the existing MSRF-based current harmonic regulation methods, the proposed scheme avoids the use of any digital filter and does not require a large amount of data storage. This approach mitigates delay effects, enhancing the dynamic performance of harmonic current regulation, and offers easy implementation. Finally, comparative experimental validation is conducted to validate the effectiveness of the proposed scheme.**

***Index Terms*—Current harmonic suppression, harmonic extraction, low pass filter (LPF)-free, multiple synchronous reference frame, permanent-magnet synchronous machine (PMSM).**

I. Introduction

PERMANENT-magnet synchronous machines (PMSMs) have been widely utilized in various applications, such as electric/hybrid vehicles, renewable energy generation, and industrial robots [1], [2]. Ensuring the high power density and high efficiency of the machine system is the goal for enhancing its performance [3], [4]. For instance, from the perspective of machine design, optimizing key structural parameters of double layer interior PMSM can enhance torque density and suppress torque ripple simultaneously [5]. Moreover, in the field of direct-drive linear motion, researchers have proposed a novel asymmetric excitation method that enables multiple magnetomotive forces, significantly enhancing force density [6]. It is noteworthy that in PMSM drive system, harmonic currents can escalate system losses, induce torque ripples, and deteriorate power quality. To cope with these problems, the approaches to reduce undesired harmonic contents in electric drives have garnered increased attention [7], [8].

In electric drive systems, harmonic currents can be broadly categorized into two groups: high-frequency harmonics and low-frequency harmonics. The high-frequency harmonics are mainly related to the switching action of power devices. By employing improved pulsewidth modulation methods [9], wide bandgap devices [10], output filters [11], high-frequency harmonic currents can be reduced. Moreover, due to the finite control bandwidth of the commonly used proportional-integral (PI) controller, periodic disturbance such as inverter nonlinearity, distorted back-electromotive force (back-EMF), parameters asymmetry, and cogging torque, etc., can lead to the low-frequency harmonics. To address this concern, several control techniques have been proposed, including resonant control [7], [12], repetitive control [13], disturbance observer [8], and multiple synchronous reference frame (MSRF) scheme [14]-[19]. Among them, the MSRF current control has garnered attention owing to its inherent simplicity and ease of expansion, positioning it as the primary focus of this paper.

The MSRF control methods treat the machine as multiple subsystems with different orders, regulating the fundamental and harmonic currents separately within several independent current loops. In this process, the low-pass filters (LPFs) are commonly employed to separate fundamental and harmonic components [14]. Typically, the cutoff frequency of LPFs is set relatively low to accurately separate the dc and harmonic components in different SRFs. However, using LPFs with a lower cutoff frequency can introduce significant delays in the control loop, which will diminish dynamic performance and affect system stability. Therefore, how to extract harmonics accurately with less negative effect on control performance is a research emphasis and has received wide attention from both academia and industry. The first-order LPF with cutoff frequency set as 5 Hz is employed in [15]. Moreover, to prevent the extracted information from being influenced by the fundamental component of phase currents, the presented harmonic extraction scheme calculates the fundamental components using the *dq*-axis current reference values and then subtracts them from the sampled phase currents. In [16], the

Z. Lyu, S. Niu, H. Zhan and K. T. Chau are with the Department of Electrical and Electronic Engineering, The Hong Kong Polytechnic University, Hong Kong, 999077, China.
T. Wang and L. Wu are with the College of Electrical Engineering, Zhejiang University, Hangzhou, 310027, China.
Corresponding author: Shuangxia Niu.

TABLE I
COMPARISON OF DIGITAL FILTERS IN EXISTING METHODS

Reference	Type of used digital filters	Cutoff frequency of LPF
[14]	LPF	2.5 Hz
[15]	first-order LPF	5 Hz
[16]	type-II Chebyshev filter	5 Hz
[17]	second-order Butterworth LPF	10 Hz
[18]	second-order LPF	Not provided
[19]	second-order LPF	5 Hz

LPFs are configured as type-II Chebyshev filters to enhance harmonic extraction performance. The designed filter, with cutoff frequency set as 5 Hz, achieves steeper roll-off compared to conventional LPFs. Furthermore, a closed-loop harmonic extraction scheme is proposed in [17], which integrates the additional PI regulators and LPFs. The presented scheme adopts the LPF cutoff frequency set to 10 Hz, and thanks to the improved detection structure, a higher detection accuracy can be attained. Experimental results demonstrate the effectiveness of these methods in extracting harmonic currents, and the MSRF-based current control scheme integrating these methods can also achieve relatively low total harmonic distortion (THD) in steady state. However, the aforementioned methods still require the use of LPFs, with the cutoff frequency set at 10 Hz or lower. Likewise, the MSRF current control can also be applied in dual three-phase PMSM for harmonic current regulation [18], [19]. TABLE I compares the used LPF and cutoff frequencies among these existing methods. Noted that the parasitic negative effects of digital filters on current control and the LPF-free harmonic control scheme are rarely investigated and merit further study.

When considering the direct separation of fundamental and harmonic currents under the MSRF framework, multiphase machines may offer a promising solution [20]. In multiphase machine drive systems, the vector space decomposition (VSD) approach can decompose the fundamental and harmonic components into multiple orthogonal subspaces. Moreover, the dimensions for harmonic separation increase as the number of machine phases increases [21]. Hence, the concept of virtual multi-three-phase system is first proposed in [22] for dual three-phase PMSMs. Specifically, a virtual pentuple three-phase system with 12° electrical degree shifting is established to directly decompose fundamental and the major current harmonics, namely the 5th, 7th, 11th, 13th harmonics, in several isolated subspaces with VSD transformation. This scheme has also been further extended to standard three-phase PMSM drive systems for 5th and 7th harmonic current regulation [23], [24]. This MSRF control scheme based on virtual windings exhibits better steady-state and transient performance than the LPF-based scheme. Nevertheless, the virtual currents are constructed by the phase shifting of measured phase currents, leading to inaccuracies in both virtual currents and detected harmonics during transient states. Additionally, this approach necessitates storing a certain amount of data for current reconstruction. Hence, these methods should further account for transient performance and implementation complexity.

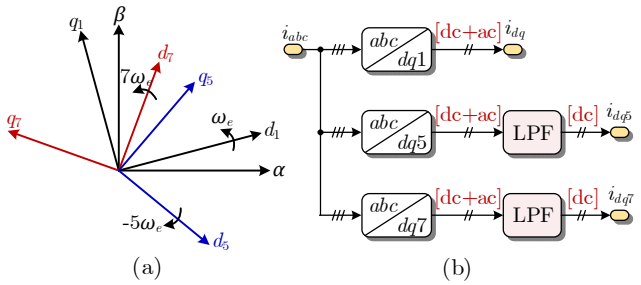

Fig. 1. MSRF-based harmonic current extraction. (a) Phasor diagram. (b) Conventional scheme using LPFs.

Considering the points mentioned above, this paper proposes a fast and effective MSRF control scheme for suppressing current harmonics for PMSM drives, the core of which is to integrate a fast harmonic extraction method. The principle and limitation of existing MSRF-based methods is analyzed firstly. Next, an enhanced harmonic extraction method based on numerical calculation is proposed for achieving the LPF-free harmonic detection. For the separation of fundamental, 5th and 7th harmonic currents, this method processes the current data at three sampling time instant during each calculation time instant, essentially performing a time-shifting operation. It enables fast and accurate extraction, allowing for independent regulation of the fundamental and harmonic currents in each subspace of MSRFs, even in transient conditions. Moreover, the general form of proposed method is also presented for arbitrary current harmonic extraction. Finally, experimental results on harmonic extraction and harmonic suppression are given to verify the effectiveness of the proposed scheme.

II. PRELIMINARIES

A. Harmonic Current Analysis

Normally, the PMSM is three-phase balanced and half-wave symmetrical, which means there are no even-order harmonics in the stator currents. Moreover, the triplen harmonics represent zero-sequence components that are not present in the stator currents of balanced Y-connected three-phase machines. Therefore, the stator currents, accounting for periodic harmonics, can be expressed as

$$\begin{bmatrix} i_a \\ i_b \\ i_c \end{bmatrix} = \underbrace{\begin{bmatrix} I_1\cos(\omega_e t+\theta_1) \\ I_1\cos(\omega_e t-2\pi/3+\theta_1) \\ I_1\cos(\omega_e t+2\pi/3+\theta_1) \end{bmatrix}}_{\text{fundamental component}} + \underbrace{\sum_{n=6k\pm1}^{\infty} \begin{bmatrix} I_n\cos(n\omega_e t+\theta_n) \\ I_n\cos(n\omega_e t-2n\pi/3+\theta_n) \\ I_n\cos(n\omega_e t+2n\pi/3+\theta_n) \end{bmatrix}}_{\text{harmonic components}} \quad (1)$$

where i_a, i_b, and i_c are three-phase currents, ω_e is the electrical angular speed, I_1 is the amplitude of the fundamental current, θ_1 is initial phase angle of the fundamental current, I_n is the amplitude of the n^{th}-order current, and θ_n is initial phase angle of the n^{th}-order harmonic component. The coordination transformation matrix which can transform components from the *a-b-c* frame to the *d-q* frame can be expressed as

$$T_{abc}^{dq} = \frac{2}{3}\begin{bmatrix} \cos\omega_e t & \cos(\omega_e t-2\pi/3) & \cos(\omega_e t+2\pi/3) \\ -\sin\omega_e t & -\sin(\omega_e t-2\pi/3) & -\sin(\omega_e t+2\pi/3) \end{bmatrix} \quad (2)$$

By applying (2), the three-phase currents in (1) can be transformed in SRF as

$$\begin{bmatrix} i_d^{SRF1} \\ i_q^{SRF1} \end{bmatrix} = \underbrace{\begin{bmatrix} I_1\cos\theta_1 \\ I_1\sin\theta_1 \end{bmatrix}}_{\text{dc component}} + \underbrace{\sum_{n=6k-1}^{\infty}\begin{bmatrix} I_n\cos[(n+1)\omega_e t+\theta_n] \\ -I_n\sin[(n+1)\omega_e t+\theta_n] \end{bmatrix} + \sum_{m=6k+1}^{\infty}\begin{bmatrix} I_m\cos[(m-1)\omega_e t+\theta_m] \\ I_m\sin[(m-1)\omega_e t+\theta_m] \end{bmatrix}}_{\text{ac components}} \quad (3)$$

where i_d^{SRF1} and i_q^{SRF1} represent the dq-axis currents in SRF rotating with the fundamental frequency.

According to (1) and (3), if without effective suppression, the stator currents include harmonics with orders of $6k\pm1$, such as 5, 7, 11, 13, etc. They can be transformed to harmonics with orders of $6k$, such as 6, 12, 18, etc. Moreover, the ones with orders of $6k$–1 are negative-sequence components and the ones with orders of $6k$+1 are positive-sequence components.

B. Basic MSRF-Based Harmonic Current Extraction and Its Limitation

The fundamental currents are represented as dc components in the SRF. Similarly, harmonic currents appear as dc components in SRFs of their corresponding rotational frequencies. This property is also used to extract harmonic currents, namely the MSRF-based harmonic current extraction, as illustrated in Fig. 1. Taking the 5th- and 7th-order harmonics as an example, the phase relationship among different SRFs is shown in Fig. 1 (a). The 5th-order SRF rotates at -5ω_e, and the 7th-order SRF rotates at 7ω_e. The corresponding coordinate transformation can be expressed as

$$T_{abc}^{dq5} = \frac{2}{3}\begin{bmatrix} \cos 5\omega_e t & \cos(5\omega_e t+2\pi/3) & \cos(5\omega_e t-2\pi/3) \\ -\sin 5\omega_e t & -\sin(5\omega_e t+2\pi/3) & -\sin(5\omega_e t-2\pi/3) \end{bmatrix} \quad (4)$$

$$T_{abc}^{dq7} = \frac{2}{3}\begin{bmatrix} \cos 7\omega_e t & \cos(7\omega_e t-2\pi/3) & \cos(7\omega_e t+2\pi/3) \\ -\sin 7\omega_e t & -\sin(7\omega_e t-2\pi/3) & -\sin(7\omega_e t+2\pi/3) \end{bmatrix} \quad (5)$$

In general, the amplitude of harmonic currents decreases as the order increases. Hence, the 5th- and 7th-order harmonic currents are usually considered to be the dominant harmonic components. Taking the case where the stator current contains the fundamental component along with the 5th- and 7th-order harmonic components for analysis, the current in the 5th-order SRF and 7th-order SRF can be expressed as

$$\begin{bmatrix} i_d^{SRF5} \\ i_q^{SRF5} \end{bmatrix} = \underbrace{\begin{bmatrix} I_5\cos\theta_5 \\ I_5\sin\theta_5 \end{bmatrix}}_{\text{dc component}} + \underbrace{\begin{bmatrix} I_1\cos(6\omega_e t+\theta_1) \\ -I_1\sin(6\omega_e t+\theta_1) \end{bmatrix} + \begin{bmatrix} I_7\cos(12\omega_e t+\theta_7) \\ -I_7\sin(12\omega_e t+\theta_7) \end{bmatrix}}_{\text{ac components}} \quad (6)$$

$$\begin{bmatrix} i_d^{SRF7} \\ i_q^{SRF7} \end{bmatrix} = \underbrace{\begin{bmatrix} I_7\cos\theta_7 \\ I_7\sin\theta_7 \end{bmatrix}}_{\text{dc component}} + \underbrace{\begin{bmatrix} I_1\cos(-6\omega_e t+\theta_1) \\ I_1\sin(-6\omega_e t+\theta_1) \end{bmatrix} + \begin{bmatrix} I_5\cos(12\omega_e t+\theta_5) \\ -I_5\sin(12\omega_e t+\theta_5) \end{bmatrix}}_{\text{ac components}} \quad (7)$$

where i_d^{SRF5} and i_q^{SRF5} represent the currents in SRF rotating with the negative 5th fundamental frequency, i_d^{SRF7} and i_q^{SRF7} represent the currents in SRF rotating with the positive 7th fundamental frequency, I_5 and I_7 represent the amplitude of the 5th and 7th order harmonic currents, respectively, θ_5 and θ_7 represent initial phase angles of two harmonic components.

Taking the 5th harmonic current in the stationary frame as an example, it appears as the dc component in its corresponding SRF. Simultaneously, the fundamental component and the 7th harmonic component appear as the 6th and 12th harmonic components respectively in this plane. Additionally, the target harmonics that have been converted into dc components can be extracted using LPFs, as depicted in Fig. 1 (b). This extraction process can be expressed as

$$\begin{bmatrix} i_{d5} \\ i_{q5} \end{bmatrix} = LPF\left(\begin{bmatrix} i_d^{SRF5} \\ i_q^{SRF5} \end{bmatrix}\right) = \begin{bmatrix} I_5\cos\theta_5 \\ I_5\sin\theta_5 \end{bmatrix} \quad (8)$$

$$\begin{bmatrix} i_{d7} \\ i_{q7} \end{bmatrix} = LPF\left(\begin{bmatrix} i_d^{SRF7} \\ i_q^{SRF7} \end{bmatrix}\right) = \begin{bmatrix} I_7\cos\theta_7 \\ I_7\sin\theta_7 \end{bmatrix} \quad (9)$$

where i_{d5}, i_{q5}, i_{d7}, and i_{q7} represent the extracted current, which can be regulated by the PI controllers later.

In recent works, first-order LPF is used in [15], and second-order Butterworth LPF is used in [17] for harmonic extraction. The transfer function of the applied filters can be expressed as

$$G_{\text{1st-order-LPF}}(s) = \frac{2\pi f_c}{s+2\pi f_c} \quad (10)$$

$$G_{\text{2nd-order-LPF}}(s) = \frac{2\pi f_c}{s^2+2\sqrt{2}\pi f_c s+(2\pi f_c)^2} \quad (11)$$

where f_c is the cutoff frequency, which is typically set at a lower frequency to ensure effective filtering of unwanted harmonics. Fig. 2 shows the amplitude-frequency characteristic of these two types of LPFs. It can be observed that the second-order LPF demonstrates better high-frequency attenuation. Nevertheless, noticeable phase lag is induced by both filters. In fact, the delay effect induced by LPFs can compromise the performance of harmonic current control, including the degradation of transient response and the difficulty of adjusting control parameters. Therefore, this paper concentrates on enhancing harmonic current suppression by introducing an LPF-free harmonic extraction method.

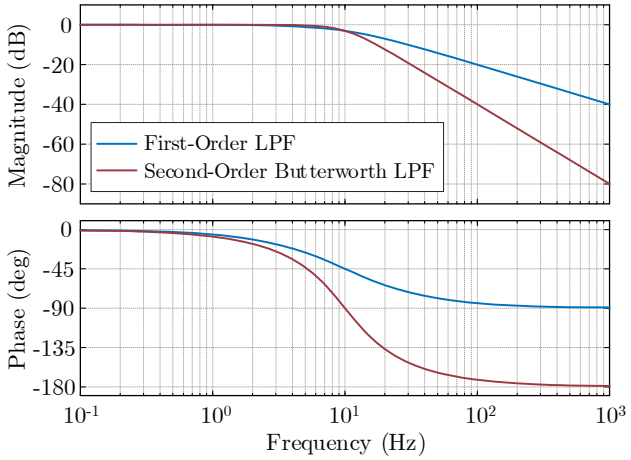

Fig. 2. Bode diagrams of two commonly used LPFs.

III. Proposed Fast Harmonic Extraction for Harmonic Current Suppression

In this section, the principle of the proposed fast harmonic extraction method is illustrated using the case of considering 5th and 7th harmonics. Moreover, the general form of extracting

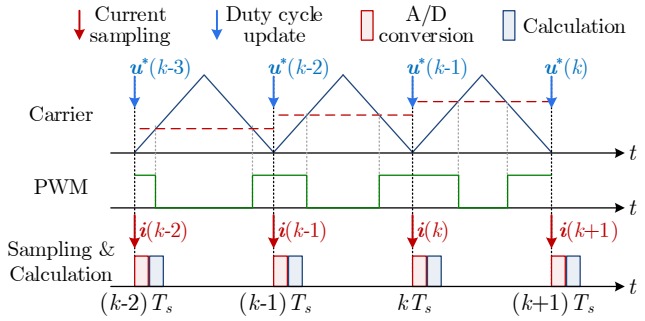

Fig. 3. Single-sampling single-update PWM with the same sampling instant and update instant.

harmonics with arbitrary orders is provided, along with the integration of proposed harmonic extraction method into the MSRF harmonic current suppression scheme.

A. Fast Harmonic Extraction Based on Time-Shifting Numerical Calculation

For the case where the stator current contains 5th and 7th harmonics, the current components of the two-phase stationary frame can be expressed as

$$\begin{bmatrix} i_\alpha \\ i_\beta \end{bmatrix} = \begin{bmatrix} I_1\cos(\omega_e t+\theta_1)+I_5\cos(5\omega_e t+\theta_5)+I_7\cos(7\omega_e t+\theta_7) \\ I_1\sin(\omega_e t+\theta_1)-I_5\sin(5\omega_e t+\theta_5)+I_7\sin(7\omega_e t+\theta_7) \end{bmatrix} \tag{12}$$

By using the concept of complex vectors, (12) can be rewritten as

$$\begin{aligned} \boldsymbol{i}_{\alpha\beta}[t] &= \boldsymbol{i}_{\alpha\beta1}[t]+\boldsymbol{i}_{\alpha\beta5}[t]+\boldsymbol{i}_{\alpha\beta7}[t] \\ &= I_1 e^{\mathrm{j}(\omega_e t+\theta_1)}+I_5 e^{-\mathrm{j}(5\omega_e t+\theta_5)}+I_7 e^{\mathrm{j}(7\omega_e t+\theta_7)} \end{aligned} \tag{13}$$

where $\boldsymbol{i}_{\alpha\beta}[t]$, $\boldsymbol{i}_{\alpha\beta1}[t]$, $\boldsymbol{i}_{\alpha\beta5}[t]$, and $\boldsymbol{i}_{\alpha\beta7}[t]$ represent the total current vector, fundamental current vector, 5th harmonic current vector, and 7th harmonic current vector, respectively.

Fig. 3 shows the timing sequence of single-sampling single-update pulsewidth modulation (PWM) scheme, where T_s is the sampling period [25]. Given that $\boldsymbol{i}_{\alpha\beta}[t]$ is known at every current sampling instant such as $t = kT_s$ and $t = (k+1)T_s$, (13) can be roughly regarded as a three-variable linear equation. From this point of view, if we want to solve for $\boldsymbol{i}_{\alpha\beta1}[t]$, $\boldsymbol{i}_{\alpha\beta5}[t]$, and $\boldsymbol{i}_{\alpha\beta7}[t]$, we would require three different equations. Assume that the currents at three consecutive sampling instants are recorded, the following equation can be obtained:

$$\begin{cases} \boldsymbol{i}_{\alpha\beta}(k) = I_1 e^{\mathrm{j}(\omega_e kT_s+\theta_1)}+I_5 e^{-\mathrm{j}(5\omega_e kT_s+\theta_5)}+I_7 e^{\mathrm{j}(7\omega_e kT_s+\theta_7)} \\ \boldsymbol{i}_{\alpha\beta}(k-1) = I_1 e^{\mathrm{j}(\omega_e kT_s-\omega_e T_s+\theta_1)}+I_5 e^{-\mathrm{j}(5\omega_e kT_s-5\omega_e T_s+\theta_5)}+I_7 e^{\mathrm{j}(7\omega_e kT_s-7\omega_e T_s+\theta_7)} \\ \boldsymbol{i}_{\alpha\beta}(k-2) = I_1 e^{\mathrm{j}(\omega_e kT_s-2\omega_e T_s+\theta_1)}+I_5 e^{-\mathrm{j}(5\omega_e kT_s-10\omega_e T_s+\theta_5)}+I_7 e^{\mathrm{j}(7\omega_e kT_s-14\omega_e T_s+\theta_7)} \end{cases} \tag{14}$$

where $\boldsymbol{i}_{\alpha\beta}(k)$, $\boldsymbol{i}_{\alpha\beta}(k\text{-}1)$, and $\boldsymbol{i}_{\alpha\beta}(k\text{-}2)$ represent the measured values at the time $t = kT_s$, $t = (k\text{-}1)T_s$, and $t = (k\text{-}2)T_s$, respectively. It should be note that only in the steady-state process, the electrical angular speed ω_e is constant. However, since the mechanical dynamic is much slower than the electrical dynamic, ω_e can be approximated as constant during successive current sampling periods [2].

The goal here is using $\boldsymbol{i}_{\alpha\beta}(k)$, $\boldsymbol{i}_{\alpha\beta}(k\text{-}1)$, $\boldsymbol{i}_{\alpha\beta}(k\text{-}2)$ to solve the current components at the calculation time instant $t = kT_s$, namely $\boldsymbol{i}_{\alpha\beta1}(k)$, $\boldsymbol{i}_{\alpha\beta5}(k)$, and $\boldsymbol{i}_{\alpha\beta7}(k)$. Hence, (14) can be rewritten as

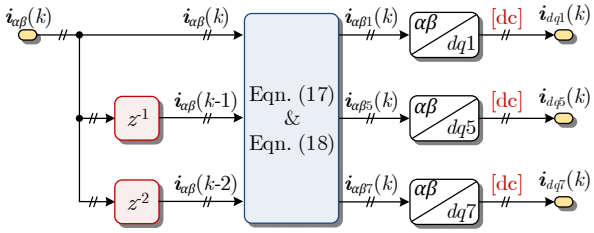

Fig. 4. Block diagram of the proposed fast current harmonic extraction.

$$\begin{bmatrix} \boldsymbol{i}_{\alpha\beta}(k) \\ \boldsymbol{i}_{\alpha\beta}(k-1) \\ \boldsymbol{i}_{\alpha\beta}(k-2) \end{bmatrix} = \boldsymbol{\Phi}\begin{bmatrix} \boldsymbol{i}_{\alpha\beta1}(k) \\ \boldsymbol{i}_{\alpha\beta5}(k) \\ \boldsymbol{i}_{\alpha\beta7}(k) \end{bmatrix} = \boldsymbol{\Phi}\begin{bmatrix} I_1 e^{\mathrm{j}(\omega_e kT_s+\theta_1)} \\ I_5 e^{-\mathrm{j}(5\omega_e kT_s+\theta_5)} \\ I_7 e^{\mathrm{j}(7\omega_e kT_s+\theta_7)} \end{bmatrix} \tag{15}$$

where $\boldsymbol{\Phi}$ represents the coefficient matrix and can be represented as

$$\boldsymbol{\Phi} = \begin{bmatrix} I & I & I \\ e^{-\mathrm{j}\omega_e T_s} & e^{\mathrm{j}5\omega_e T_s} & e^{-\mathrm{j}7\omega_e T_s} \\ e^{-\mathrm{j}2\omega_e T_s} & e^{\mathrm{j}10\omega_e T_s} & e^{-\mathrm{j}14\omega_e T_s} \end{bmatrix} \tag{16}$$

It can be seen that $\boldsymbol{\Phi}$ is related to $\omega_e T_s$, that is, the electrical angle the rotor rotates during one current sampling period. Then, the fundamental, 5th, and 7th current vector at the time $t = kT_s$, can be obtained as

$$\begin{bmatrix} \boldsymbol{i}_{\alpha\beta1}(k) \\ \boldsymbol{i}_{\alpha\beta5}(k) \\ \boldsymbol{i}_{\alpha\beta7}(k) \end{bmatrix} = \boldsymbol{\Phi}^{-1}\begin{bmatrix} \boldsymbol{i}_{\alpha\beta}(k) \\ \boldsymbol{i}_{\alpha\beta}(k-1) \\ \boldsymbol{i}_{\alpha\beta}(k-2) \end{bmatrix} \tag{17}$$

To avoid directly performing matrix inversion and to reduce the computational burden of the digital controller, the expression for the inverse matrix of $\boldsymbol{\Phi}$ is further given by

$$\boldsymbol{\Phi}^{-1} = \frac{1}{\det(\boldsymbol{\Phi})}\begin{bmatrix} e^{-\mathrm{j}9\omega_e T_s}-e^{-\mathrm{j}3\omega_e T_s} & e^{\mathrm{j}10\omega_e T_s}-e^{-\mathrm{j}14\omega_e T_s} & e^{-\mathrm{j}7\omega_e T_s}-e^{\mathrm{j}5\omega_e T_s} \\ e^{\mathrm{j}9\omega_e T_s}-e^{-\mathrm{j}15\omega_e T_s} & e^{\mathrm{j}14\omega_e T_s}-e^{-\mathrm{j}2\omega_e T_s} & e^{-\mathrm{j}\omega_e T_s}-e^{-\mathrm{j}7\omega_e T_s} \\ e^{\mathrm{j}9\omega_e T_s}-e^{\mathrm{j}3\omega_e T_s} & e^{\mathrm{j}2\omega_e T_s}-e^{\mathrm{j}10\omega_e T_s} & e^{\mathrm{j}5\omega_e T_s}-e^{-\mathrm{j}\omega_e T_s} \end{bmatrix} \tag{18}$$

It is evident that the inverse of coefficient matrix can be relatively easily obtained by calculating the determinant and adjugate matrix.

The above method realizes the separation of fundamental and major harmonic currents from a numerical calculation standpoint. Then, the currents extracted by the above process can be converted into $\boldsymbol{i}_{dq1}$, $\boldsymbol{i}_{dq5}$, and $\boldsymbol{i}_{dq7}$ by corresponding Park transformations. Fig. 4 depicts the block diagram of the proposed fast harmonic extraction scheme. The entire process makes full use of the phase angle relationship between harmonics with different orders and realizes harmonic current extraction without LPF. In addition, since only the current information of three adjacent sampling points is needed under ideal conditions, the enhanced performance can be achieved, particularly under transient conditions.

B. General Form of Proposed Harmonic Extraction for Arbitrary Current Harmonics

The aforementioned expression is derived based on the PMSM with 5th and 7th harmonic currents, which are two of the most common harmonics. Due to various non-ideal factors in the inverter and machine, the harmonic components in the electric drive system can manifest at any order. To broaden the

applicability of the proposed harmonic extraction technique, the general form for separating harmonics with arbitrary order is provided below.

$$\boldsymbol{i}_{\alpha\beta}[t]=\boldsymbol{i}_{\alpha\beta1}[t]+\boldsymbol{i}_{\alpha\beta\gamma}[t]=I_1e^{\mathrm{j}(\omega_e t+\theta_1)}+I_\gamma e^{\mathrm{j}(\gamma\omega_e t+\theta_\gamma)} \tag{19}$$

where γ represents the harmonic order. To extract the γ^{th}-order harmonics from the $\boldsymbol{i}_{\alpha\beta}[t]$, the currents at two consecutive sampling instants are recorded, and can be represented as

$$\begin{cases}\boldsymbol{i}_{\alpha\beta}(k)=I_1e^{\mathrm{j}(\omega_e kT_s+\theta_1)}+I_\gamma e^{\mathrm{j}(\gamma\omega_e kT_s+\theta_\gamma)}\\ \boldsymbol{i}_{\alpha\beta}(k-1)=I_1e^{\mathrm{j}(\omega_e kT_s-\omega_e T_s+\theta_1)}+I_\gamma e^{\mathrm{j}(\gamma\omega_e kT_s-\gamma\omega_e T_s+\theta_\gamma)}\end{cases} \tag{20}$$

The goal here is using $\boldsymbol{i}_{\alpha\beta}(k)$ and $\boldsymbol{i}_{\alpha\beta}(k\text{-}1)$ to solve the current components at the calculation time instant $t=kT_s$, namely $\boldsymbol{i}_{\alpha\beta1}(k)$ and $\boldsymbol{i}_{\alpha\beta\gamma}(k)$. Hence, (20) can be rewritten as

$$\begin{bmatrix}\boldsymbol{i}_{\alpha\beta}(k)\\ \boldsymbol{i}_{\alpha\beta}(k-1)\end{bmatrix}=\boldsymbol{\Phi}_{Gen}\begin{bmatrix}\boldsymbol{i}_{\alpha\beta1}(k)\\ \boldsymbol{i}_{\alpha\beta\gamma}(k)\end{bmatrix}=\boldsymbol{\Phi}_{Gen}\begin{bmatrix}I_1e^{\mathrm{j}(\omega_e kT_s+\theta_1)}\\ I_\gamma e^{\mathrm{j}(\gamma\omega_e kT_s+\theta_\gamma)}\end{bmatrix} \tag{21}$$

where $\boldsymbol{\Phi}_{Gen}$ represent the general coefficient matrix and can be expressed as

$$\boldsymbol{\Phi}_{Gen}=\begin{bmatrix}I & I\\ e^{-\mathrm{j}\omega_e T_s} & e^{-\mathrm{j}\gamma\omega_e T_s}\end{bmatrix} \tag{22}$$

Therefore, the fundamental and γ^{th}-order harmonic current vector at the calculation time instant $t=kT_s$ can be obtained as

$$\begin{aligned}\begin{bmatrix}\boldsymbol{i}_{\alpha\beta1}(k)\\ \boldsymbol{i}_{\alpha\beta\gamma}(k)\end{bmatrix}&=\boldsymbol{\Phi}_{Gen}^{-1}\begin{bmatrix}\boldsymbol{i}_{\alpha\beta}(k)\\ \boldsymbol{i}_{\alpha\beta}(k-1)\end{bmatrix}\\ &=\frac{1}{e^{-\mathrm{j}\gamma\omega_e T_s}-e^{-\mathrm{j}\omega_e T_s}}\begin{bmatrix}e^{-\mathrm{j}\gamma\omega_e T_s}\boldsymbol{i}_{\alpha\beta}(k)-\boldsymbol{i}_{\alpha\beta}(k-1)\\ -\boldsymbol{i}_{\alpha\beta}(k)+e^{-\mathrm{j}\omega_e T_s}\boldsymbol{i}_{\alpha\beta}(k-1)\end{bmatrix}\end{aligned} \tag{23}$$

Noted that for the separation of harmonic currents with different orders, the parameter design does not exhibit substantial discrepancies. The primary focus involves the adjustment of a coefficient matrix that pertains to the harmonic order. Hence, in line with the majority of existing harmonic extraction and control schemes, the proposed scheme necessitates prior knowledge of the harmonic order.

C. Harmonic Current Suppression Scheme with Fast Harmonic Extraction

The fast harmonic extraction method based on time-shifting numerical calculation is presented, including an explicit form for the 5th and 7th harmonics and a general form for harmonics of arbitrary order. In this subsection, the proposed harmonic extraction method will be integrated into the MSRF harmonic current control scheme to achieve effective harmonic suppression.

Taking the case of suppressing the 5th and 7th harmonics as an example, the coefficient matrix for separating the harmonics is shown in (18). Noted that the derivation is based on that the stator currents at three consecutive sampling instants are recorded and used for calculation. That is to say, ideally, even in transient processes, the harmonics can be extracted after two sampling periods. The coefficients in (16) and (18) can be seen to be composed of $\sin(n^*\omega_eT_s)$ and $\cos(n^*\omega_eT_s)$, where n represents positive integers. Fig. 5 illustrates the relationship between these coefficients and variations in rotor speed, while also providing the magnitude of determinant, denoted as

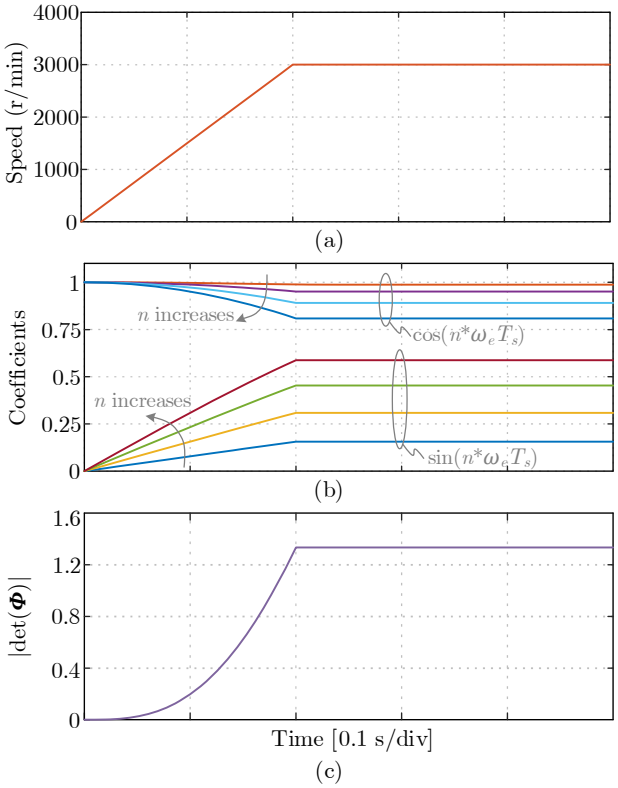

Fig. 5. Relationship between matrix coefficients for harmonic extraction and rotor speed variation. (a) Speed. (b) Coefficients. (c) Magnitude of Determinant.

$|\det(\boldsymbol{\Phi})|$. It is shown that when the rotor speed is not zero, that is, when ω_e is not zero, the determinant of the matrix is non-zero, indicating that $\boldsymbol{\Phi}$ is invertible. At the same time, this also means that when the rotor speed is zero during operation, the proposed strategy needs to be disabled. Moreover, when the speed is relatively low, the values of a cluster of coefficients associated with the sine function and $|\det(\boldsymbol{\Phi})|$ tend to be relatively small. In numerical computations, due to round-off errors and limitations in finite precision, this situation can result in inaccuracies or instability in the computed results, making the calculation challenging or unreliable. In order to avoid the occurrence of extremely small values in the harmonic-separating matrix, the harmonic extraction method can be optimized in time according to the rotor speed. Specifically, when the PMSM is running at low speed, switch from using $\boldsymbol{i}_{\alpha\beta}(k)$, $\boldsymbol{i}_{\alpha\beta}(k\text{-}T_s)$, and $\boldsymbol{i}_{\alpha\beta}(k\text{-}2T_s)$ for harmonic current extraction to using $\boldsymbol{i}_{\alpha\beta}(k)$, $\boldsymbol{i}_{\alpha\beta}(k\text{-}\lambda T_s)$, and $\boldsymbol{i}_{\alpha\beta}(k\text{-}2\lambda T_s)$, where λ is positive integer and is adjusted according to ω_e. A smaller coefficient λ indicates faster harmonic extraction, while a larger coefficient corresponds to the improved extraction accuracy. The value of λ can be finely adjusted according to the specific microcontroller in use and the precision demands of the application scenario.

Fig. 6 displays the overall diagram of the proposed harmonic current suppression approach with fast harmonic extraction. It employs the widely adopted speed-current cascade structure. The PI controller serves as the speed regulator, while the maximum torque per ampere (MTPA) block is employed to compute the fundamental dq-axis reference currents $\boldsymbol{i}_{dq1}^*$. The

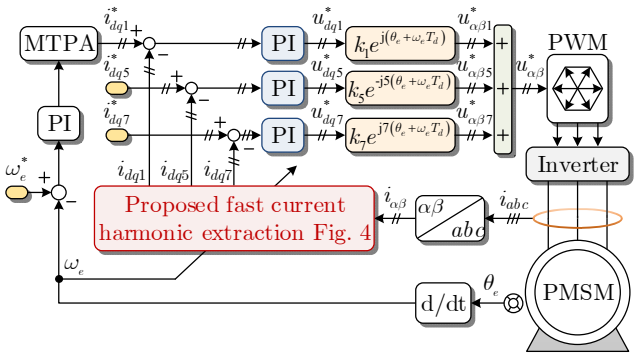

Fig. 6. Diagram of the proposed harmonic current suppression scheme based on fast harmonic extraction.

current loop is implemented through the studied approach, integrating the MSRF current controller and the proposed fast harmonic extraction. The presented solution can be regarded as an improved MSRF harmonic current regulation scheme, which treats the PMSM as multiple subsystems with different orders, enabling independent current control of fundamental and harmonics separately. Moreover, in comparison to the conventional MSRF control methods, the proposed scheme achieves LPF-free operation and mitigates delay effects. Noted that the coefficient λ can update according to the changes in the rotor speed. As for harmonic current reference, the reference values $\boldsymbol{i}^*_{dq5}$ and $\boldsymbol{i}^*_{dq7}$ of the harmonic plane are set to zero to suppress the harmonics. They can also be optimized to realized harmonic injection with the proposed scheme for specific objectives. Since the major harmonics are decomposed, the current components in each subspace of MSRF are approximately expressed as dc components and can be regulated by PI controllers. The transfer function of current controller in the γ^{th}-order subspace can be expressed as

$$G_{c\gamma}(s) = k_{p\gamma} + \frac{k_{i\gamma}}{s} \tag{24}$$

where $k_{p\gamma}$ and $k_{i\gamma}$ represent the proportional gain and integral part, respectively. The parameters are designed according to [26] can be represented as

$$k_{p\gamma} = \omega_{c\gamma} L_{s\gamma},\ k_{i\gamma} = \omega_{c\gamma} R_{s\gamma} \tag{25}$$

where $\omega_{c\gamma}$ represents the cutoff frequency of the γ^{th}-order current loop, and $L_{s\gamma}$ and $R_{s\gamma}$ are stator inductance and resistance in the γ^{th} SRF. Since the proposed harmonic separation strategy avoids the use of LPFs, the delay induced within the current loop is almost negligible. Consequently, the expected bandwidth and cutoff frequency of each plane can be designed to be the same. Then, the output of current controllers, namely u^*_{dq1}, u^*_{dq5}, and u^*_{dq7}, can be transformed into the $\alpha\beta$ stationary frame. Moreover, the impact of the frame rotation during the digital delay can introduce errors in the voltage output, which is particularly noticeable for the current regulation within the rapidly rotating SRFs [27]. Specifically, digital delay can lead to discrepancies between the voltages generated by current controller and the actual voltages applied to the PMSM. Hence, the voltage error compensation is integrated with the inverse Park transformations of each SRFs, which can be expressed as

$$\boldsymbol{u}^*_{\alpha\beta\gamma} = k_\gamma e^{j\gamma(\theta_e + \omega_e T_d)} \boldsymbol{u}^*_{dq\gamma} = k_\gamma e^{j\gamma(\theta_e + 1.5\omega_e T_s)} \boldsymbol{u}^*_{dq\gamma} \tag{26}$$

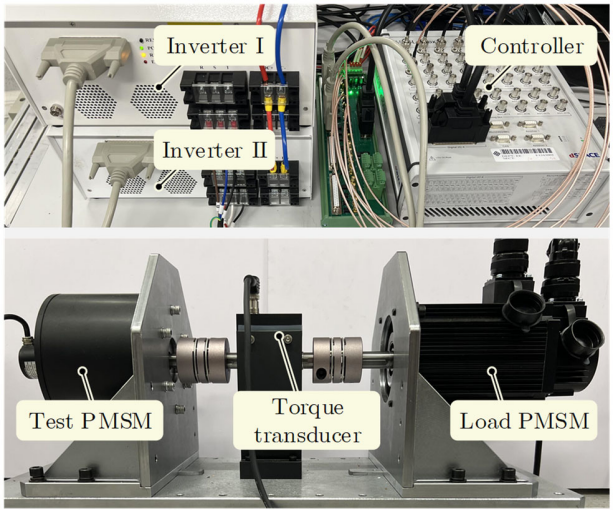

Fig. 7. Experimental setup.

TABLE II
PARAMETERS OF THE TEST PMSM

Parameter	Value	Parameter	Value
Pole pairs	5	Rated current (A)	4.25
Rated speed (r/min)	1200	d-axis inductance L_d (mH)	2.20
Stator resistance R_s (Ω)	0.6	q-axis inductance L_q (mH)	2.20

$$k_\gamma = \frac{\gamma \omega_e T_s}{2\sin(0.5\gamma\omega_e T_s)} \tag{27}$$

where T_d represents the delay time and is approximately equal to $1.5T_s$ [25]. Finally, the reference voltage values yielded by each plane are aggregated to derive the total reference voltage, represented as:

$$\boldsymbol{u}^*_{\alpha\beta} = \boldsymbol{u}^*_{\alpha\beta 1} + \boldsymbol{u}^*_{\alpha\beta 5} + \boldsymbol{u}^*_{\alpha\beta 7} \tag{28}$$

Through time-shifting harmonic extraction, this scheme effectively transfers the regulation of a specific harmonic into the closed-loop control of a set of two dc components. It can aim in suppressing the 5th and 7th harmonics resulting from back-EMF distortion and inverter nonlinearity, which are prevalent in PMSM drive systems. Moreover, it could also be extended to suppress harmonic currents with arbitrary orders.

IV. Experimental Validation

A. Test Bench Setup

To validate the proposed method, experimental results are conducted on a setup depicted in Fig. 7. The overall control scheme is executed on a dSPACE MicroLabBox. Both the test PMSM and the load PMSM are each driven by a three-phase inverter. The switching frequency of the inverters and the current sampling frequency are both set to 10 kHz. Main parameters of the test PMSM are detailed in TABLE II.

B. Steady-State Performance

To illustrate the operating principle of the proposed scheme more clearly, Fig. 8 displays the waveforms of $\alpha\beta$-axes currents at three sampling instants, kT_s, $(k\text{-}2)T_s$, and $(k\text{-}4)T_s$, corresponding to the scenario with $\lambda = 2$. The speed of test PMSM is 800 r/min and the peak value of the phase current is

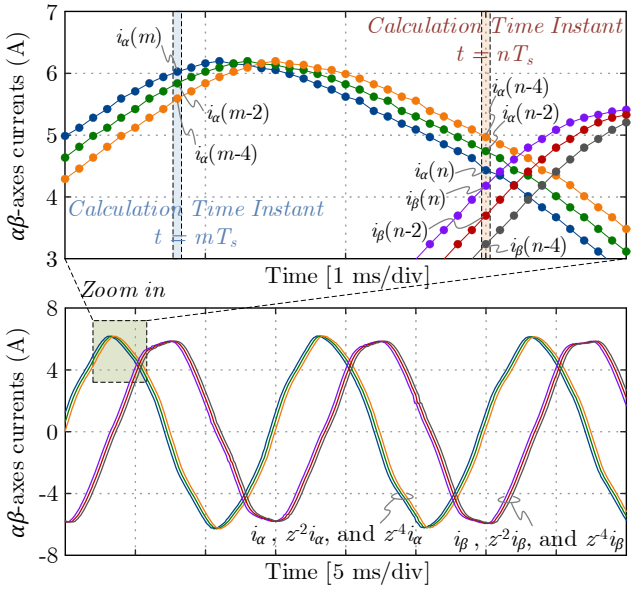

Fig. 8. Waveforms of $\alpha\beta$-axes currents at three sampling instants: kT_s, $(k\text{-}2)T_s$, and $(k\text{-}4)T_s$ with zoom-in view.

about 6 A. It should be noted that, at this time, only the harmonic detection method is utilized, while the harmonic current suppression method remains inactive. As can be seen, there are obvious harmonic components in the $\alpha\beta$-axes current waveforms. Moreover, to realize the proposed harmonic extraction method, the current information of three sampling instants is recorded and displayed. At each calculation time constant, in addition to the stator current information at the present time, the information from the two prior sampling instants is also incorporated. The interval between the used sampling instants is denoted by λT_s and $2\lambda T_s$. Specifically, using $\boldsymbol{i}_{\alpha\beta}(n)$, $\boldsymbol{i}_{\alpha\beta}(n\text{-}2)$, $\boldsymbol{i}_{\alpha\beta}(n\text{-}4)$ can further allow for the decomposition of the fundamental current and dominant harmonic currents at the calculation time instant $t = nT_s$, so as to obtain $\boldsymbol{i}_{\alpha\beta 1}(n)$, $\boldsymbol{i}_{\alpha\beta 5}(n)$, and $\boldsymbol{i}_{\alpha\beta 7}(n)$.

To validate the efficacy of harmonic current reduction, steady-state current performance of conventional field-oriented control (FOC) and proposed control scheme under different speeds is presented and compared in Fig. 9 and Fig. 10. The results of phase currents, dq-axis currents, and the harmonic spectrum of phase-A current are displayed. Noted that as for the proposed control scheme, the dq-axis currents derived from the conventional Park transformation are only employed for comparative purposes and do not contribute to the closed-loop control. Regarding Fig. 9, the reference speed is set as 600 r/min, representing a 50% rated speed condition, and the peak value of phase current is around 3 A. As shown in Fig. 9 (a), under conventional FOC, the phase current waveforms exhibit obvious distortion, primarily stemming from the harmonics present in the back-EMFs. Additionally, there are periodic ripples observed in the dq-axis currents. The fast Fourier transform spectrum reveals that the phase current comprises prominent 5th and 7th harmonics, with magnitudes amounting to 2.52% and 0.91% of the fundamental current component, respectively. The THD stands at 3.75%. In contrast, as depicted

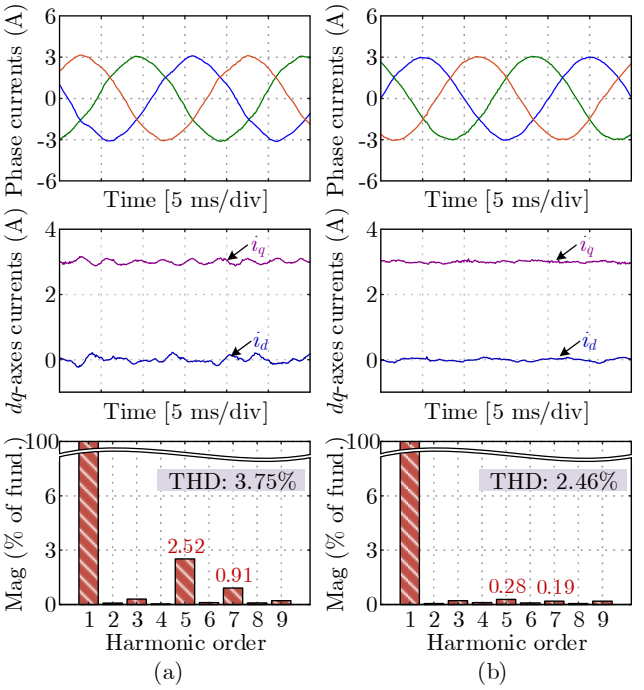

Fig. 9. Experimental results of stator currents under 600r/min. (a) Conventional FOC. (b) Proposed scheme.

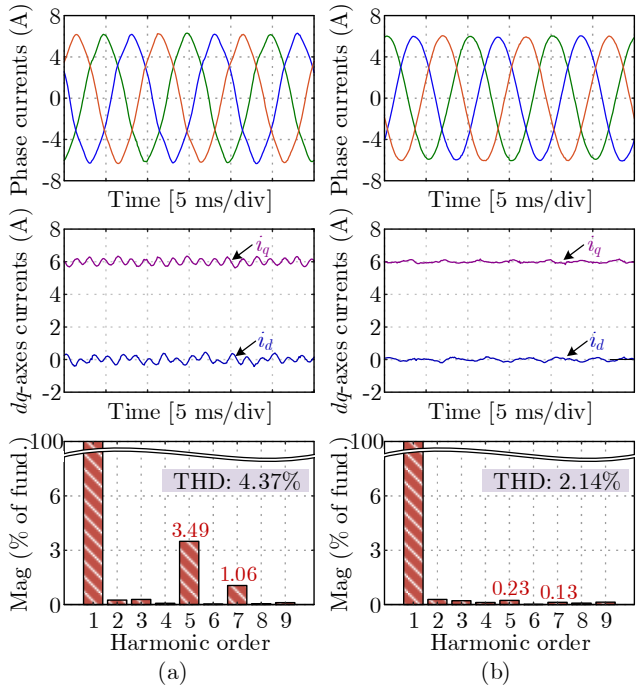

Fig. 10. Experimental results of stator currents under 1200r/min. (a) Conventional FOC. (b) Proposed scheme.

in Fig. 9 (b), the proposed scheme effectively suppresses the undesirable harmonics in both the phase currents and dq-axis currents. The magnitudes of the 5th and 7th harmonics can be decreased to 0.28% and 0.19% of the fundamental current component, respectively. Consequently, the THD of phase current can be decreased to 2.46%. Moreover, Fig. 10 depicts the experimental results with the reference speed is set as 1200 r/min, representing a 100% rated speed condition, and the peak

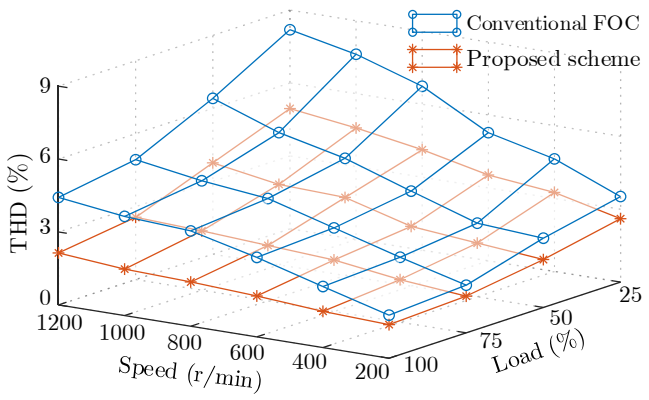

Fig. 11. Experimental comparison results of THD under different speed and load conditions.

value of phase current is around 6 A, corresponding to the rated load conditions. As the speed increases, the harmonic voltage disturbance induced by back-EMFs also increases. Furthermore, the rise in the motor operating frequency increases the frequencies linked with the 5th and 7th harmonics in phase currents, making them more difficult for conventional PI controllers to track, consequently amplifying the amplitudes of these harmonics. However, as depicted in Fig. 10 (b), the proposed scheme demonstrates the ability to effectively suppress the primary harmonics to a notably low level, resulting in a reduction of the THD from 4.37% to 2.14%.

To highlight the efficacy of the proposed method across various operational scenarios, Fig. 11 presents the experimental comparison results of THD values under different speed and load conditions. The current distortion tends to rise with increasing speed and decreasing load, aligning with theoretical analysis. Furthermore, the proposed strategy consistently exhibits notable harmonic suppression effects across all working conditions.

C. Dynamic Performance

As aforementioned, digital filters like LPFs are frequently employed in existing MSRF current control methods. The delay effect caused by LPFs can undermine the efficacy of harmonic current control, leading to issues such as degraded transient response and challenges in adjusting control parameters. For verifying the efficacy and superiority of the proposed LPF-free MSRF control scheme, experiments are conducted to compare it with LPF-based MSRF control method.

Fig. 12 shows the experimental results under the current step response. The waveforms of phase currents and dq-axis currents with conventional FOC, LPF-based MSRF control, and the proposed scheme are given respectively. Referring to the existing MSRF work [14]-[17], the second-order LPFs with cutoff frequency set as 10 Hz are adopted. For conducting a fair evaluation, the same PI controller parameters are set across all three methods, with k_p = 6 and k_i = 1500. In experiments, the reference speed is set as 600 r/min, while the q-axis current is approximately stepped from 2 A to 5 A. As shown in Fig. 12 (a), since the conventional FOC cannot effectively suppress the harmonics, the phase current before and after the current step has obvious distortion. The q-axis current ripple, i.e., the peak-to-peak value, in the steady state before and after the current step are approximately 0.32 A and 0.38 A, respectively. Notably, within a brief timeframe subsequent to the current step, the q-axis current ripple increases to 0.57 A. Moreover, as shown in Fig. 12 (b), the LPF-based current control method can effectively reduce the current harmonics in steady-state conditions. The q-axis current ripple in the steady state before and after the current step are approximately 0.23 A and 0.24 A, respectively. Nevertheless, the bandwidth of the harmonic control loop diminishes due to the LPF-induced delay. Consequently, the q-axis current ripple surges to 0.55 A within a short period after the current step. In contrast, as depicted in Fig. 12 (c), the proposed control scheme can effectively suppress harmonic currents in both steady state and transient state. Specifically, the q-axis current ripple in the steady state is further mitigated, decreasing to approximately 0.14 A before and 0.16 A after the current step. In particular, even during the transient period following the step response, the q-axis current ripple remains low at only 0.22 A, showcasing that the proposed method can achieve a smaller setting time for regulating harmonic currents.

By and large, the proposed control scheme shows decent performance in suppressing harmonic currents under multiple operating conditions.

D. Computational Burden Performance

The execution time of conventional FOC, LPF-based MSRF control, and the proposed scheme are compared in Fig. 13. The conventional FOC has no harmonic extraction link and employs two PI controllers in the current loop, so the total execution time is only 13.8 μs. Moreover, both the LPF-based MSRF control method and the proposed method incorporate the harmonic extraction link and utilize six PI controllers in the current loop, leading to longer execution times of 22.1 μs and 26.9 μs respectively. This disparity signifies that the proposed method achieves better harmonic suppression capability at the expense of increased execution time. Nevertheless, given a PMSM drive system with a control frequency of 10 kHz, where each execution cycle spans 100 μs, the actual execution time of the proposed method remains within acceptable limits.

V. Discussion

In addition to machine drive systems, low-frequency harmonic current issues are prevalent in grid-connected inverter applications as well [28], [29]. In general, the harmonic current regulation includes determining the reference of harmonics and effective harmonic control methods. This paper concentrates on harmonic extraction and regulation utilizing the MSRF scheme, and successfully achieving harmonic current suppression in PMSM drives through the adjustment of the harmonic reference value to zero. There are still several points to consider regarding the presented approach.

First, the regulation of harmonic current requires the injection of a specific harmonic voltage, thus it is crucial to consider the inverter voltage constraint as highlighted in [18], [19], and [24]. Second, the harmonic current suppression typically targets

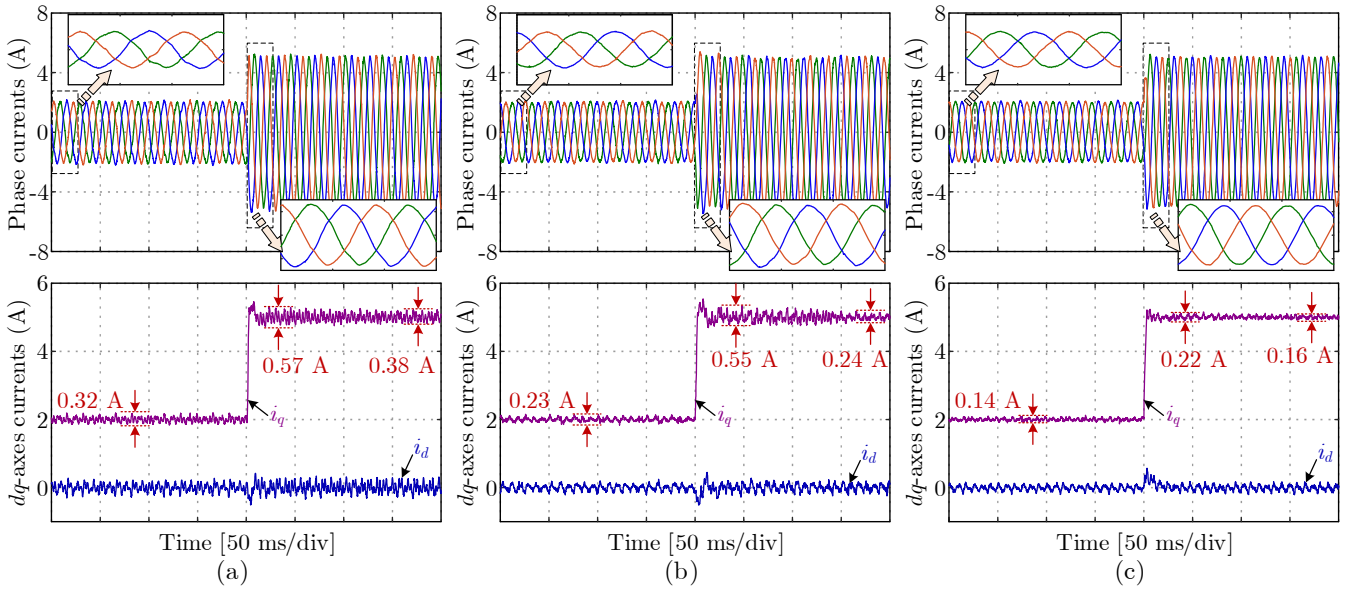

Fig. 12. Experimental results with load torque changes. (a) Conventional FOC. (b) LPF-based MSRF current control. (c) Proposed scheme.

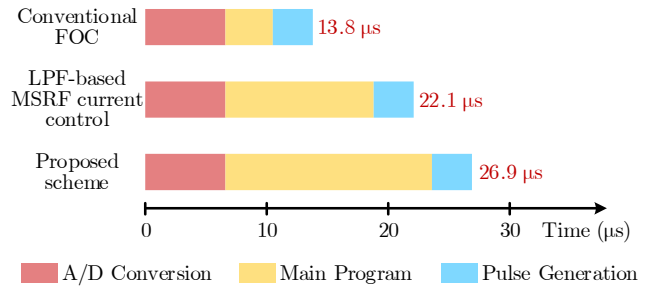

Fig. 13. Comparison of execution time among three methods.

achieving sinusoidal stator current and decreasing system losses. In PMSM drive systems, appropriate harmonic current injection can achieve further performance improvements, like mitigating torque ripple [30]-[32]. After determining the optimized harmonic current reference, using the harmonic extraction and regulation scheme proposed in this paper can facilitate effective harmonic current injection.

VI. Conclusion

In this paper, the limitation of the conventional MSRF current control with LPFs is illustrated. It is found that the LPF for harmonic extraction introduces significant delay, thereby constraining control effectiveness. To solve this key issue, a rapid and efficient MSRF scheme with LPF-free solution is proposed. Notably, a fast harmonic extraction method is introduced based on time-shifting numerical calculation. For the separation of fundamental, 5^{th} and 7^{th} harmonic currents, only the stator current data from three sampling instants is needed. The general form of proposed harmonic extraction for arbitrary current harmonics is also presented. The proposed method involves using a small amount of historical current data to extract harmonics with reduced delay, thereby fostering high-performance harmonic current regulation. Experimental results demonstrate efficacy and superiority of this approach.

References

[1] K. T. Chau, C. C. Chan and C. Liu, "Overview of permanent-magnet brushless drives for electric and hybrid electric vehicles," *IEEE Trans. Ind. Electron.*, vol. 55, no. 6, pp. 2246-2257, Jun. 2008.

[2] M. Yang, X. Lang, J. Long and D. Xu, "Flux immunity robust predictive current control with incremental model and extended state observer for PMSM drive," *IEEE Trans. Power Electron.*, vol. 32, no. 12, pp. 9267-9279, Dec. 2017.

[3] I. Husain *et al.*, "Electric drive technology trends, challenges, and opportunities for future electric vehicles," *Proceedings of the IEEE*, vol. 109, no. 6, pp. 1039-1059, Jun. 2021.

[4] Z. Li and S. Niu, "A double-sided complementary Vernier PM linear machine with high magnet utilization factor using third-order harmonics," *IEEE Trans. Ind. Electron.*, vol. 71, no. 9, pp. 11217-11228, Sep. 2024.

[5] L. Dai, J. Gao, S. Niu and S. Huang, "Multi-electromagnetic performance optimization of double-layer interior permanent magnet synchronous machine," *IEEE Trans. Ind. Electron.*, vol. 71, no. 11, pp. 14535-14545, Nov. 2024.

[6] Y. Shen, Z. Li, Z. Zeng, Q. Lu and C. H. T. Lee, "Quantitative analysis of asymmetric flux reversal permanent magnet linear machine for long excursion application," *IEEE Trans. Ind. Electron.*, vol. 71, no. 10, pp. 12781-12792, Oct. 2024.

[7] H. Kim, Y. Han, K. Lee and S. Bhattacharya, "A sinusoidal current control strategy based on harmonic voltage injection for harmonic loss reduction of PMSMs with non-sinusoidal back-EMF," *IEEE Trans. Ind. Appl.*, vol. 56, no. 6, pp. 7032-7043, Nov.-Dec. 2020.

[8] M. Hu, W. Hua, C. Cheng, Y. Wang and C. Lu, "Discrete-time frequency-domain disturbance observer to mitigate harmonic current in PMSM drives and the implementation with reduced delay," *IEEE Trans. Power Electron.*, vol. 38, no. 8, pp. 9482-9493, Aug. 2023.

[9] A. Birda, J. Reuss and C. M. Hackl, "Synchronous optimal pulsewidth modulation for synchronous machines with highly operating point dependent magnetic dnisotropy," *IEEE Trans. Ind. Electron.*, vol. 68, no. 5, pp. 3760-3769, May. 2021.

[10] A. K. Morya *et al.*, "Wide bandgap devices in AC electric drives: Opportunities and challenges," *IEEE Trans. Transport. Electrific.*, vol. 5, no. 1, pp. 3-20, Mar. 2019.

[11] Z. Lyu and L. Wu, "Resonant frequency deviation analysis and modified notch filter-based active damping for SiC-based PMSM drive with sine wave filter," *IEEE Trans. Energy Convers*, vol. 38, no. 1, pp. 417-427, Mar. 2023.

[12] C. Xia, B. Ji and Y. Yan, "Smooth speed control for low-speed high-torque permanent-magnet synchronous motor using

proportional-integral-resonant controller," *IEEE Trans. Ind. Electron.*, vol. 62, no. 4, pp. 2123-2134, Apr. 2015.
[13] M. Tian, B. Wang, Y. Yu, Q. Dong and D. Xu, "Discrete-time repetitive control-based ADRC for current loop disturbances suppression of PMSM drives," *IEEE Trans. Ind. Informat.*, vol. 18, no. 5, pp. 3138-3149, May. 2022.
[14] E. Uz-Logoglu, O. Salor and M. Ermis, "Online characterization of interharmonics and harmonics of AC electric arc furnaces by multiple synchronous reference frame analysis," *IEEE Trans. Ind. Appl.*, vol. 52, no. 3, pp. 2673-2683, May-June 2016.
[15] Z. Chen, T. Shi, Z. Lin, Z. Wang and X. Gu, "Analysis and control of current harmonic in IPMSM field-oriented control system," *IEEE Trans. Power Electron.*, vol. 37, no. 8, pp. 9571-9585, Aug. 2022.
[16] W. Wang, C. Liu, S. Liu, Z. Song, H. Zhao and B. Dai, "Current harmonic suppression for permanent-magnet synchronous motor based on Chebyshev filter and PI controller," *IEEE Trans. Magn.*, vol. 57, no. 2, pp. 1-6, Feb. 2021.
[17] G. Liu, B. Chen, K. Wang, and X. Song, "Selective current harmonic suppression for high-speed PMSM based on high-precision harmonic detection method," *IEEE Trans. Ind. Informat.*, vol. 15, no. 6, pp. 3457-3468, Jun. 2019.
[18] J. Karttunen, S. Kallio, J. Honkanen, P. Peltoniemi and P. Silventoinen, "Partial current harmonic compensation in dual three-phase PMSMs considering the limited available voltage," *IEEE Trans. Ind. Electron.*, vol. 64, no. 2, pp. 1038-1048, Feb. 2017.
[19] G. Feng, C. Lai, W. Li, Z. Li and N. C. Kar, "Dual reference frame based current harmonic minimization for dual three-phase PMSM considering inverter voltage limit," *IEEE Trans. Power Electron.*, vol. 36, no. 7, pp. 8055-8066, July 2021.
[20] E. Levi, "Multiphase electric machines for variable-speed applications," *IEEE Trans. Ind. Electron.*, vol. 55, no. 5, pp. 1893-1909, May 2008.
[21] I. Zoric, M. Jones, and E. Levi, "Vector space decomposition algorithm for asymmetrical multiphase machines," in *Proc. Int. Symp. Power Electron.*, Oct. 2017, pp. 1-6.
[22] L. Yan *et al*., "Suppression of major current harmonics for dual three-phase PMSMs by virtual multi three-phase systems," *IEEE Trans. Ind. Electron.*, vol. 69, no. 6, pp. 5478-5490, Jun. 2022.
[23] Z. Lyu, L. Wu, J. Yi and S. Yang, "Hybrid frame-based current control scheme for *LC*-equipped PMSM with non-sinusoidal back-EMF," *IEEE Trans. Power Electron.*, vol. 38, no. 5, pp. 5994-6004, May. 2023.
[24] Z. Lyu, L. Wu and P. Song, "A novel harmonic current control method for torque ripple reduction of SPMSM considering DC-link voltage limit," *IEEE Trans. Power Electron.*, vol. 39, no. 2, pp. 2558-2568, Feb. 2024.
[25] S. Buso and P. Mattavelli, *Digital Control in Power Electronics*. San Rafael, CA, USA: Morgan & Claypool, 2015.
[26] S. Yang and K. Lin, "Automatic control loop tuning for permanent-magnet AC servo motor drives," *IEEE Trans. Ind. Electron.*, vol. 63, no. 3, pp. 1499-1506, Mar. 2016.
[27] Bon-Ho Bae and S. -K. Sul, "A compensation method for time delay of full-digital synchronous frame current regulator of PWM AC drives," *IEEE Trans. Ind. Appl.*, vol. 39, no. 3, pp. 802-810, May-Jun. 2003.
[28] D. Campos-Gaona, R. Peña-Alzola, J. L. Monroy-Morales, M. Ordonez, O. Anaya-Lara and W. E. Leithead, "Fast selective harmonic mitigation in multifunctional inverters using internal model controllers and synchronous reference *IEEE Trans. Ind. Electron.*, vol. 64, no. 8, pp. 6338-6349, Aug. 2017.
[29] P. Shan, Y. Sun, Y. Song, F. Zhang, Y. Li and K. Sun, "Adaptive parameter tuning and virtual impedance injection control for coupled harmonic mitigation of photovoltaic converter," *IEEE Trans. Power Electron.*, vol. 40, no. 1, pp. 162-175, Jan. 2025.
[30] G. Feng, C. Lai and N. C. Kar, "An analytical solution to optimal stator current design for PMSM torque ripple minimization with minimal machine losses," *IEEE Trans. Ind. Electron.*, vol. 64, no. 10, pp. 7655-7665, Oct. 2017.
[31] Y. Ma, S. Niu, W. Fu and J. Fei, "A novel direct-drive rotary-linear machine and ripple reduction by harmonic current injection approach," *IEEE Trans. Power Electron.*, vol. 38, no. 12, pp. 15272-15286, Dec. 2023.
[32] V. Varvolik *et al*., "Comparative study on torque ripple reduction considering minimum losses for synchronous reluctance motor drives," *IEEE Trans. Transport. Electrific.*, vol. 10, no. 3, pp. 6527-6538, Sep. 2024.

Zekai Lyu (Member, IEEE) received the B.Eng. degree from Southwest Jiaotong University, Chengdu, China, in 2018, the M.Sc. degree from Harbin Institute of Technology, Harbin, China, in 2020, and the Ph.D. degree from Zhejiang University, Hangzhou, China, in 2024, all in electrical engineering.

He is currently a Postdoctoral Fellow with the Department of Electrical and Electronic Engineering, The Hong Kong Polytechnic University, Hong Kong SAR, China. His research interests include wide-bandgap device applications, electrical machines, and machine drives.

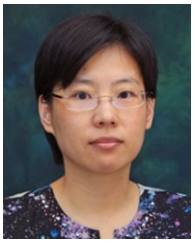

Shuangxia Niu (Senior Member, IEEE) received the B.Sc. and M.Sc. degrees in electrical engineering from Tianjin University, China, in 2002 and 2005, respectively, and the Ph.D. degree from The University of Hong Kong, Hong Kong, in 2009.

She is currently working as Professor with the Department of Electrical and Electronic Engineering, The Hong Kong Polytechnic University, Hong Kong. Her research interests include the electric vehicle technologies, renewable energy systems, machines and drives, power electronics technology, applied electromagnetic, numerical method and optimization.

Haolan Zhan (Student Member, IEEE) received the B.Eng. and M.Sc. degrees in electrical engineering from Zhejiang University, Hangzhou, China, in 2020 and 2023, respectively. From 2023 to 2024, he was a research assistant with the College of Electrical Engineering, Zhejiang University.

He is currently working toward the Ph.D. degree in Department of Electrical and Electronic Engineering with The Hong Kong Polytechnic University, Hong Kong, China. His major research interests include fault diagnosis and fault-tolerant control of permanent magnet machines.

Tao Wang (Senior Member, IEEE) received the B.Eng. and the Ph.D. degrees both from the College of Electrical Engineering, Zhejiang University, Hangzhou, China, in July 2013 and June 2018, respectively. From 2018 to 2020, he worked as a Postdoc Research Associate in the electronic and electrical engineering department of the University of Sheffield, U.K. From 2020 to 2023, he was with Nanjing University of Aeronautics and Astronautics, Nanjing, China, where he worked as an Associate Professor in the college of automation engineering. Since 2024, he has been a Research Professor with the College of Electrical Engineering, Zhejiang University, Hangzhou, China.

His current research interests include wind power generation, aviation power supply, permanent magnet synchronous machine control, and model predictive control.

Lijian Wu (Senior Member, IEEE) received the B.Eng. and M.Sc. degrees from Hefei University of Technology, Hefei, China, in 2001 and 2004, respectively, and the Ph.D. degree from the University of Sheffield, Sheffield, U.K., in 2011, all in electrical engineering.

From 2004 to 2007, he was an Engineer with Delta Electronics (Shanghai) Co, Ltd. From 2012 to 2013, he was with Sheffield Siemens Wind Power Research Center as a design engineer focusing on wind power generators. From 2013 to 2016, he was an advanced engineer with Siemens Wind Power A/S, Brande, Denmark. Since 2016, he has been with Zhejiang University, where he is currently a Professor of electrical machines and control systems. His current major research interests include design and control of permanent magnet machines.

K.T. Chau (Fellow, IEEE) received the B.Sc. (Eng.), M.Phil., and Ph.D. degrees in electrical and electronic engineering from The University of Hong Kong, Hong Kong, China, in 1988, 1991, and 1993, respectively.

He serves as a Chair Professor in electrical energy engineering with the Research Centre for Electric Vehicles and Department of Electrical and Electronic Engineering, The Hong Kong Polytechnic University. His research interests include electric and hybrid vehicles, power electronics and drives, and renewable energies. He is the author of nine books and more than 350 journal papers. Prof. Chau is a Fellow of the Institution of Engineering and Technology (IET), U.K., and the Hong Kong Institution of Engineers. He is also a Co-Editor of the Journal of Asian Electric Vehicles. He is a Chartered Engineer. He was the recipient of the Changjiang Chair Professorship from the Ministry of Education, China, and the Environmental Excellence in Transportation Award for Education, Training, and Public Awareness from the Society of Automotive Engineers International.